Generation of sub-30-fs microjoule mid-infrared pulses for ultrafast vibrational dynamics at solid/liquid interfaces

Abdelaziz Boulesbaa, Oleksandr Isaienko, Aashish Tuladhar, and Eric Borguet*

Department of Chemistry, Temple University, 1901 North 13th Street, Philadelphia, Pennsylvania 19122, USA
**Corresponding author: eborguet@temple.edu*

Received May 3, 2013; accepted June 6, 2013;
posted August 14, 2013 (Doc. ID 189965); published November 21, 2013

We describe temporal compression of ultrabroadband, few microjoule mid-infrared (mid-IR) pulses from a noncollinear optical parametric amplifier (NOPA) employed in a sum-frequency generation (SFG) vibrational spectroscopic system, operating in total-internal-reflection geometry. The propagation of the mid-IR beam through optical materials results in a significant temporal chirp at the probed interface, which is analyzed and corrected by properly managing the total dispersion of materials introduced into the mid-IR beam path. By employing the simultaneous spatial and temporal focusing of the broadband infrared pulses at the probed interface, we achieve a sub-50-fs full width at half-maximum (FWHM) for the instrument response function, measured via SFG cross correlation of the ultrashort mid-IR pulses with an ultrashort (~30 fs) near-IR pulse from a synchronized, independently tunable NOPA. From the SFG cross-correlation FWHM, we extract a sub-30-fs mid-IR pulse duration, making it a suitable SFG spectroscopic system to investigate vibrational dynamics in hydrogen-bonded systems at interfaces.

OCIS codes: (190.7110) Ultrafast nonlinear optics; (320.2250) Femtosecond phenomena; (320.5520) Pulse compression.
http://dx.doi.org/10.1364/OL.38.005008

Understanding ultrafast interactions in solids and condensed molecular systems requires the use of ultrashort laser pulses [1–4]. In particular, ultrashort mid-infrared (mid-IR) pulses of microjoule/pulse energies are indispensable for studies of the ultrafast dynamics of vibrational energy flow in hydrogen-bonded networks [1,2], where vibrational spectral diffusion in the OH stretch modes in liquid water has been reported to occur on a 50 fs timescale [1]. The investigation of such ultrafast phenomena has been facilitated to a large extent by the development of optical parametric amplifiers (OPAs), enabling the generation of ultrashort pulses tunable in a wide spectral range [5]. The dispersion properties of certain nonlinear optical materials, such as potassium titanyl phosphate (KTP), lithium niobate (LNB), potassium niobate (KNB), and periodically poled stoichiometric lithium tantalate ($LiTaO_3$), provide conditions for group-velocity matching between near-infrared (NIR) signal ($\lambda_s \sim 1000$–1600 nm) and mid-IR idler ($\lambda_i \sim 1600$–4000 nm) pulses when pumped at the fundamental wavelength of Ti:sapphire lasers, thus allowing broadband phase matching in the corresponding wavelength ranges [6,7]. Such conditions have been implemented, in particular, in KNB to generate ~45 fs pulses around 3000 nm [8]. Using specially engineered poled nonlinear optical materials, generation of ~25 fs pulses at 3600 nm was reported [7]. Other recent advancements in the generation of ultrashort mid-IR pulses include the application of aperiodic phase matching [9], as well as developments in mid-IR optical parametric chirped pulse amplification [10].

Recently, we demonstrated broadband amplification of NIR and mid-IR pulses in a noncollinear OPA (NOPA) based on a two-stage amplification of white-light continuum in LNB and KNB crystals [11,12]. These pulses have been applied to the vibrational sum-frequency generation (SFG) spectroscopy at solid/liquid interfaces [11]. SFG is highly surface sensitive due to the fact that second-order nonlinear optical effects are forbidden in centrosymmetric environments (in the electric dipole approximation). This property confines the generation of the nonlinear response to the interfacial layer, where the inversion symmetry is naturally lost. Frequently, SFG is carried out in total-internal-reflection geometry [11], which provides a significant increase in the SFG signal levels. However, in this geometry the broadband infrared pulses unavoidably pass through relatively large thicknesses (≥10 mm) of the investigated solid material, in addition to the collimating/focusing optics. This typically introduces temporal chirp into the broadband infrared pulses, which has to be corrected in order to investigate ultrafast vibrational dynamics with the highest possible temporal resolution.

In this paper, we demonstrate compression of the mid-IR idler pulses from a LNB–KNB NOPA at the surface of the mineral fluorite (CaF_2) by compensating the overall dispersion caused by the optics in the spectroscopic setup, and by employing the simultaneous spatial and temporal focusing (SSTF) developed earlier for microscopy [13]. The combination of the dispersion compensation and SSTF allows us to temporally compress the broadband mid-IR idler pulses at the focal point of the idler beam [13], even though it possesses a pulse-front tilt due to the NOPA process [11]. In order to perform time-resolved SFG spectroscopy on an ultrashort timescale, we built a second NOPA that is synchronized with the mid-IR NOPA and generates ultrashort NIR (~1500 nm) pulses. The instrument response has a FWHM of ~47 fs, suggesting that the infrared pulses have sub-30-fs duration at the probed interface.

The experimental setup for the generation of sub-30-fs mid-IR pulses and SFG spectroscopy is depicted in Fig. 1. The laser source is a Ti:sapphire oscillator (MIRA,

Coherent) regeneratively amplified with a BMI Thales (Alpha 1000) laser system operating in femtosecond mode as described elsewhere [14]. The fundamental pulse is centered at 800 nm with 150 fs pulse duration at 1 kHz repetition rate, and energy of 600 μJ per pulse. The regenerative amplifier (Regen) output is used to pump two NOPAs; NOPA1 is used to generate ultrashort mid-IR pulses and NOPA2 to generate ultrashort NIR pulses. The beam transmitted through BS1 (Fig. 1) is used for mid-IR pulse generation as described previously [11]. Briefly, NOPA1 is based on the ultrabroadband amplification of the near-IR portion of the white-light continuum (WLC) from sapphire in two consecutive NOPA stages [11,12]. The first stage is based on a 2 mm thick congruent LNB crystal (Type I, cut at $\theta = 48°$), while the second stage is based on a KNB crystal (2.5 mm thick, Type I, cut at $\theta = 38°$) [11]. The external noncollinear pump-seed angle at the second stage is reduced to 3° (~1.5° internal) in order to decrease angular dispersion in the mid-IR idler output while maintaining the broad bandwidth of the NOPA.

To characterize the broadband mid-IR pulses in the time domain, we constructed NOPA2 based on broadband Type II amplification of WLC from 800 nm pumped sapphire in KTP [6]. By setting the external noncollinear angle between the WLC seed and the 800 nm pump to ~7° and the internal pump beam phase-matching angle close to ~49° [6], we achieve ultrabroadband amplification of near-IR pulses in the 1100–1600 nm range from the KTP NOPA [6].

The signal from NOPA2 was collimated using a 250 mm CaF_2 lens (L1), and residual WLC was filtered out using two silicon wafers (Si-w in Fig. 1, 1 mm total thickness). The collimated signal of NOPA2 was temporally compressed using two Brewster angle (69.6°) fused silica prisms separated by a distance of 310 mm. The dispersion in the signal of NOPA2 caused by propagation through KTP, Si-w, L1, L2, and the CaF_2 prism was compensated for by adjusting the distance between P1 and P2 and the beam insertion in P1 and P2. The compressed NIR pulse was sent through a motorized delay stage before it was focused (100 μm spot size) with a 100 mm CaF_2 lens (L2) onto the CaF_2/Au interface at a 65° angle of incidence.

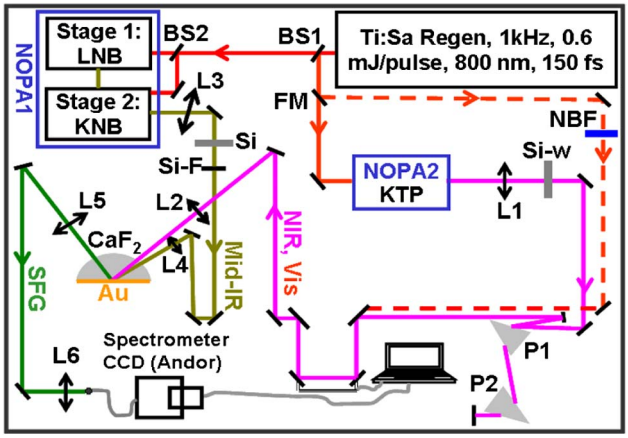

Fig. 1. Experimental setup: BS, beam splitters (BS1 and BS2, 60% transmission; BS3, 90% transmission); FM, flip-mounted mirror; WP, half-wave plate; L, lenses; Sa, sapphire window; NBF, narrowband filter; Si-w, silicon wafers; P, 69.6°-apex angle fused silica prisms; Si, 5 mm thick IR coated silicon window; Si-F, 1 mm thick silicon long-pass filter; CaF_2, hemi-cylinder prism.

The mid-IR idler beam from NOPA1 was collimated by a 50 mm CaF_2 lens (L3), and passed through a 1 mm thick silicon-based long-pass filter (Si-F) to suppress the residual signal and WLC after the second stage. For mid-IR pulse temporal compression, a 5 mm thick IR anti-reflection-coated Si window (Si) was introduced into the optical path. The NOPA1 mid-IR pulses were overlapped with the upconverting pulses (either 800 nm or NIR signal from NOPA2) at the flat surface of a CaF_2 hemicylinder prism coated with ~100 nm thick gold film (Fig. 1) [2,11]. The mid-IR beam was focused onto the interface using a 50 mm CaF_2 lens (L4) at a 73° angle of incidence. The NIR-SFG field was generated at the CaF_2/Au interface by upconversion of mid-IR pulses with NIR pulses. NOPA2 was tuned to ~1500 nm so that the NIR-SFG was redshifted to ~1000 nm from the 800 nm fundamental wavelength that inevitably leaked into the detection system. To measure the mid-IR pulse spectra, we used the 800 nm output of the Regen to upconvert the mid-IR pulses into the visible by SFG (Vis-SFG, 615–655 nm spectral range) as indicated by the dotted line in Fig. 1. For better spectral resolution, the 800 nm beam passed through a narrowband filter (NBF) to spectrally narrow it down to ~2 nm [15]. Pulse energies at the sample were 4, 2, and 10 μJ for mid-IR, NIR, and 800 nm pulses, respectively.

The Vis-SFG or NIR-SFG (depending on the experiment) beam was collimated and refocused into a 200 μm core fiber coupled to a spectrograph–CCD (Andor Shamrock/iDus) detection system. The NIR-SFG cross-correlation traces were recorded at different delays using a custom built program based on LabVIEW software (National Instruments). Using half-wave plates and polarizers, the SFG, the NIR, the 800 nm, and the mid-IR were *p*-polarized relative to the interface.

Initial measurements of the mid-IR pulse spectra [Fig. 2(a)] were done with only 1 mm of silicon (Si-F in Fig. 1) and 20 mm total of CaF_2 (L3, L4, and prism of the sample) in the mid-IR beam path before reaching the interface. The "blue" edge in the mid-IR spectrum [–660 fs plot in Fig. 2(a)] was upconverted into the Vis-SFG field before the "red" edge [+660 fs plot in Fig. 2(a)], suggesting that the broadband mid-IR pulse was temporally chirped. In the case of unchirped mid-IR pulses, Vis-SFG spectra are expected to be observed with the same central frequency when the time delay changes within the duration of the upconverting pulse. The effective mid-IR pulse duration was ~1 ps measured from FWHM of the intensity-integrated Vis-SFG cross correlation.

The chirp is in part the consequence of the materials (2.5 mm KNB crystal, a 5 mm thick CaF_2 collimation lens (L3), a 1 mm thick Si-F, a 2 mm thick CaF_2 focusing lens (L4), and a 13 mm radius hemi-cylindrical CaF_2 prism, Fig. 1), through which the mid-IR pulses pass before reaching the interface [16]. The mid-IR pulse is spectrally broad, spanning ~1000 cm^{-1} (FWHM = 660 cm^{-1}). As a result of its propagation through 20 mm of CaF_2, "blue" frequencies reach the interface earlier compared to "red" frequencies due to the accumulated dispersion in

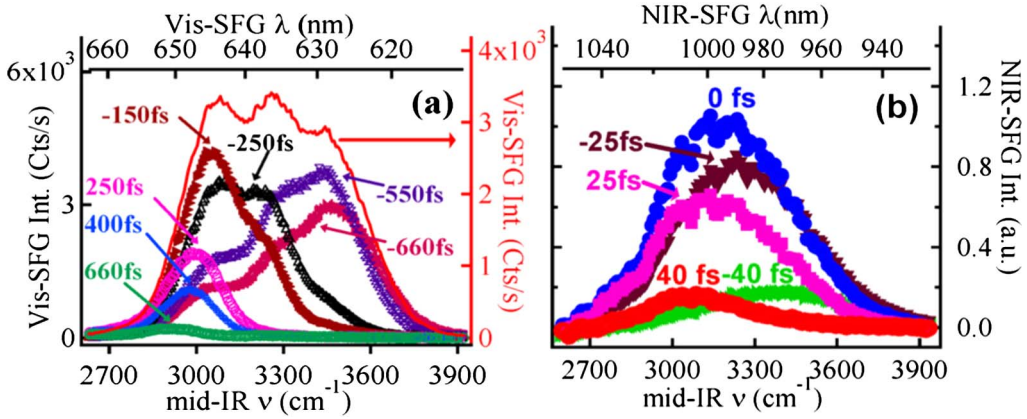

Fig. 2. (a) Vis-SFG spectra (symbol plots) obtained at different time delays (as indicated) and without the 5 mm Si window in the mid-IR optical path. Solid line shows the Vis-SFG spectrum obtained at a single time delay and with the 5 mm thick Si window introduced into the mid-IR beam path. (b) NIR-SFG spectra obtained at different time delays (as indicated) and with the 5 mm thick Si window introduced into the mid-IR beam path.

the broadband pulses, indicating negatively chirped mid-IR pulses. We quantified this temporal chirp by plotting the relative delay center of mass ($CoM_{Vis\text{-}SFG}$) of the Vis-SFG response at each frequency [Fig. 3(a)].

The chirp in a broad mid-IR pulse centered at 3250 cm^{-1}, and covering the range 2750–3750 cm^{-1}, was simulated up to the fourth order in a Taylor series expansion of the phase, $\phi(\omega)$, of the pulse around the central frequency, ω_0, by calculating the group delay $\tau(\omega) = d\phi(\omega)/d\omega$ [17]. The dispersion in the mid-IR pulses caused by propagation through 2.5 mm of KNB and 20 mm of CaF_2 material [CaF_2 + KNB plot in Fig. 3(a)] is qualitatively in agreement with the experimentally observed negative chirp [$CoM_{Vis-SFG}$ plot in Fig. 3(a)]. Quantitatively, the small disagreement between the simulation and experiment likely reflects chirp due to angular dispersion and pulse front tilt in the mid-IR pulse generated from NOPA1 [11]. Under the experimental conditions (internal noncollinear angle ~1.5° and mid-IR beam diameter ~2 mm), the presence of a pulse-front tilt in the mid-IR pulses can potentially lead to a temporal elongation on the order of ~1 ps [11]. The good agreement between the experimental $CoM_{Vis\text{-}SFG}$ and the calculated CaF_2 + KNB plots in Fig. 3(a) suggests that the chirp due to angular dispersion and pulse front tilt is much smaller than the estimated value (~1 ps). A possible reason for the decrease of the chirp caused by angular dispersion and pulse front tilt is the implementation of SSTF [13]. The SSTF concept is based on the temporal compression of the front-tilted pulses at the focal point, with the condition that the pulse has minimum dispersion [13].

To investigate the possibility of compensating for the temporal chirp resulting from the propagation of the mid-IR pulse through optical components before reaching the interface, the effect of 6 mm of silicon (Si and Si-F in Fig. 1) on the mid-IR pulse was simulated [Si plot in Fig. 3(a)]. The dotted and dashed lines in Fig. 3(a) show that the total dispersion induced by KNB and CaF_2 has the opposite sign to that of silicon. The sum of the two effects [net chirp plot in Fig. 3(a)] produces a net chirp in the mid-IR pulse that is negligible over the "blue" side of the spectrum. However, the "red" frequency components are expected to be delayed by up to ~150 fs.

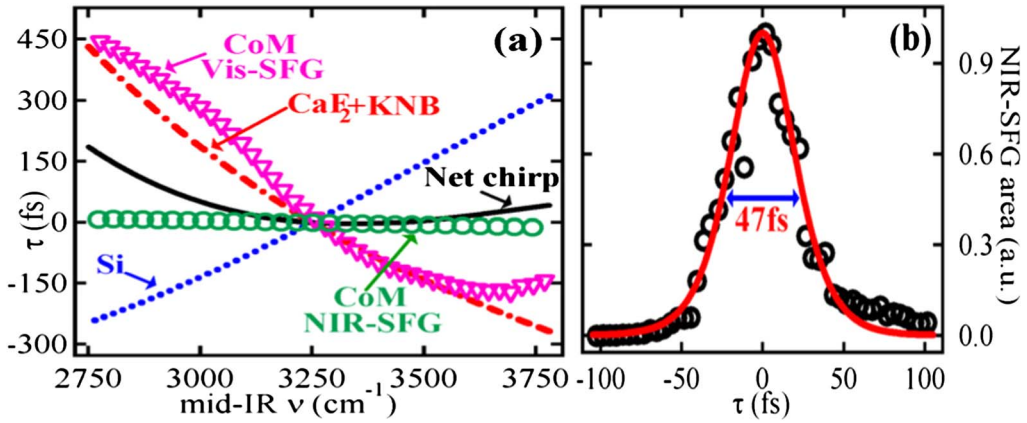

Fig. 3. (a) Simulated group delay (τ) in a mid-IR pulse centered at 3250 cm^{-1} after propagation in 2.5 mm thick KNB and 20 mm thick CaF_2 (dashed line), and 6 mm thick Si (dotted line). The solid line is a sum of the two effects. Triangles represent the delay-center of mass (CoM) of Vis-SFG spectra shown in Fig. 2(a), i.e., before the silicon plate was added. Open circles represent the CoM of NIR-SFG spectra shown in Fig. 2(b), i.e., after the silicon plate is inserted. (b) NIR-SFG cross correlation plotted as integrated intensity of NIR-SFG spectra versus time delay between the compressed mid-IR and the NIR pulses.

After placing a 5 mm thick silicon window ("Si" in Fig. 1) into the optical path of mid-IR beam, the Vis-SFG spectrum [solid-line in Fig. 2(a)] at a zero time delay τ, contained all the frequencies in the symbol plots combined, indicating compensation of the temporal chirp in the mid-IR pulse by the Si window that has opposite dispersion compared to CaF_2 and KNB [17].

The time-domain characterization of the compressed mid-IR pulses was performed via NIR-SFG [Fig. 2(b)] with ultrashort near-IR signal pulses from NOPA2. The spectrum of the signal output of NOPA2 (not shown here) was obtained via second-harmonic generation at the CaF_2/Au interface. The NOPA2 signal has a central wavelength of ~1500 nm and a spectral bandwidth of 125 nm, corresponding to a transform-limited duration of ~20 fs (~3.7 optical cycles), assuming a $sech^2$ shaped pulse. The optimization of the NIR pulse duration was done by adjusting the P1–P2 prism compressor to find the shortest cross correlation of the mid-IR and NIR pulses at the probed interface of the CaF_2 prism.

The experimental cross correlation, measured via integration of NIR-SFG spectral intensity as a function of delay τ between the NIR and mid-IR pulses, recorded from the CaF_2/Au interface is fit well with a $sech^2$ function yielding FWHM $= 47 \pm 2.6$ fs [Fig. 3(b)]. If we assume that the NIR and mid-IR pulsewidths are similar, the obtained FWHM for the NIR-SFG cross correlation suggests that NIR and mid-IR pulse durations are ~27 fs, assuming $sech^2$ shaped pulses. However, since the shortest NIR duration achieved was 38 fs (data not shown here) measured by β-barium borate (BBO)-based intensity autocorrelation and prism pair dispersion compensation in P1–P2, the experimentally obtained FWHM for NIR-SFG cross correlation [Fig. 3(b)] suggests that the mid-IR may be shorter than 27 fs. Such a short mid-IR pulse duration, for a pulse expected to be front tilted, demonstrates that SSTF was implemented in our spectroscopic setup.

Although the mid-IR and NIR pulses were compressed down to the sub-30-fs regime, the temporal chirp was not completely canceled out: a fraction of the "blue" frequency components of the mid-IR pulse [−40 fs plot in Fig. 2(b)] were upconverted into NIR-SFG field before "red" components [+40 fs plot in Fig. 2(b)]. This is expected based on the simulated net chirp shown in Fig. 3(a). Quantitatively, the delay center of mass of the NIR-SFG spectra [$CoM_{NIR\text{-}SFG}$ plot in Fig. 3(a)] reflects much less chirp due to the fact that the intensities at the peaks of NIR-SFG spectra at −40 fs and +40 fs delays are less than 20% of the intensity at 0 fs delay.

In conclusion, a spectroscopic system producing and employing sub-30-fs mid-IR pulses is described. Our mid-IR NOPA is based on nonlinear optical crystals in their bulk forms, which simplifies its design and the phase-matching calculations compared to OPAs based on poled materials [7,10]. The mid-IR idler pulses were compressed close to the transform limit by combining the compensation of the optical dispersion (by introducing the appropriate amount of Si into the IR beam path) with SSTF [13]. The current instrument enables vibrational SFG spectroscopy of CaF_2/aqueous interfaces on a sub-50-fs time scale. Such temporal resolution is suitable, in particular, to probe the ultrafast vibrational dynamics in hydrogen-bonded networks at fluorite/liquid interfaces. We believe that the technique can be extended to other relevant interfaces, such as metal and semiconductor oxides in contact with aqueous media, by properly compensating for the dispersion of the bulk material through which the ultrabroadband pulses pass.

The authors acknowledge the National Science Foundation (CHE 1337880) for support of this research.

References

1. M. L. Cowan, B. D. Bruner, N. Huse, J. R. Dwyer, B. Chugh, E. T. J. Nibbering, T. Elsaesser, and R. J. D. Miller, Nature **434**, 199 (2005).
2. A. Eftekhari-Bafrooei and E. Borguet, J. Am. Chem. Soc. **131**, 12034 (2009).
3. N. A. Anderson and T. Lian, Annu. Rev. Phys. Chem. **56**, 491 (2005).
4. J. B. Asbury, T. Steinel, C. Stromberg, K. J. Gaffney, I. R. Piletic, A. Goun, and M. D. Fayer, Phys. Rev. Lett. **91**, 237402 (2003).
5. D. Brida, C. Manzoni, G. Cirmi, M. Marangoni, S. Bonora, P. Villoresi, S. De Silvestri, and G. Cerullo, J. Opt. **12**, 013001 (2010).
6. O. Isaienko and E. Borguet, Opt. Express **16**, 3949 (2008).
7. D. Brida, M. Marangoni, C. Manzoni, S. De Silvestri, and G. Cerullo, Opt. Lett. **33**, 2901 (2008).
8. C. J. Fecko, J. J. Loparo, and A. Tokmakoff, Opt. Commun. **241**, 521 (2004).
9. C. Heese, C. R. Phillips, L. Gallmann, M. M. Fejer, and U. Keller, Opt. Lett. **35**, 2340 (2010).
10. O. Chalus, P. K. Bates, M. Smolarski, and J. Biegert, Opt. Express **17**, 3587 (2009).
11. O. Isaienko and E. Borguet, Opt. Express **20**, 547 (2012).
12. O. Isaienko and E. Borguet, J. Opt. Soc. Am. B **30**, 2075 (2013).
13. G. Zhu, J. van Howe, M. Durst, W. Zipfel, and C. Xu, Opt. Express **13**, 2153 (2005).
14. D. Bodlaki and E. Borguet, Rev. Sci. Instrum. **71**, 4050 (2000).
15. A. Lagutchev, A. Lozano, P. Mukherjee, S. A. Hambir, and D. D. Dlott, Spectrochim. Acta A **75**, 1289 (2010).
16. M. Daimon and A. Masumura, Appl. Opt. **41**, 5275 (2002).
17. N. Demirdöven, M. Khalil, O. Golonzka, and A. Tokmakoff, Opt. Lett. **27**, 433 (2002).